Steady-State Diagnostic Model of Summer Mean Circulation on the Georgia Shelf

THOMAS N. LEE

*Division of Meteorology and Physical Oceanography, School of Marine and Atmospheric Science,
University of Miami, Miami, FL 33149*

ERNEST DADDIO

Evans Hamilton, Inc., Rockville, MD 20850

GREGORY C. HAN[1]

Atlantic Oceanographic and Meteorological Laboratories, NOAA, Miami, FL 33149

(Manuscript received 25 September 1981, in final form 12 April 1982)

ABSTRACT

The Galt (1975) diagnostic model was used to investigate summer circulation on the Georgia shelf. The steady-state model uses a finite-element method to solve the depth-integrated vorticity equation for sea surface elevation over the model domain from which horizontal transports are derived. Good agreement was found between predicted and observed flows for the mid-shelf region, between the 20 and 40 m isobaths. The model was not applicable to the outer shelf due partly to the transient occurrence of Gulf Stream meanders and eddies that produced large spatial and temporal variations in the density and flow fields; and partly to the rapid depth changes in the continental slope region which made it difficult to resolve horizontal gradients of the vertical averaged density.

The model was used to estimate a net northward along-shelf volume transport of 70×10^3 m^3 s^{-1} over the model domain for the six-day averaging period. Along-shelf transport was primarily barotropic below the pycnocline and a mixture of Ekman plus barotropic modes above the pycnocline. Net cross-shelf transport was estimated at 40×10^3 m^3 s^{-1} offshore, due mostly to offshore Ekman transport in the upper layer. This cross-shelf transport is equivalent to a net exchange rate and was used to estimate a shelf residence time of 3.8 months.

1. Introduction

The determination of the velocity and mass transport fields over a continental shelf region requires a larger set of current measurements than is normally practical to obtain. However, with hydrographic station data and a small number of current meters, one can use numerical modeling techniques to enhance estimates of velocity and transport fields.

A steady-state diagnostic vorticity balance model was used to study summer circulation on the Georgia shelf. This model was first used and described in detail by Galt (1975) and Galt and Watabayshi (1977). It incorporates the forcing functions of the imposed surface wind stress, density field and surface slope, and accounts for the interaction of the velocity field with variable bottom topography.

Data requirements for the model include a grid of STD stations to compute the density field, water depth at each station, and wind measurements, to derive the local wind stress. Current meter records are used to verify the model results and to estimate the sea surface slope boundary conditions. The equations of motion are simplified by dropping time-dependent terms, thus making the equations diagnostic and steady-state. The flow modeled is relatively slow so that nonlinear terms are neglected and friction is considered to be important only in the surface and bottom layers.

The model is here used to depict shelf mean flow conditions which occur on time scales of two weeks or longer. Thus the effects of tidal, wind and Gulf Stream forcing, which occur on time scales of less than two weeks (Lee and Brooks, 1979; Lee et al., 1981) are not accounted for. The model results will be degraded to the extent that the effect of these processes alias the measured density field.

2. Model formulation

A detailed derivation and discussion of the model can be found in Galt (1975) and Galt and Watabayashi (1977). A discussion of the finite-element

solution procedure was made by Galt (1980) and a recent application of the model to the New York Bight was made by Han et al. (1980). A brief review of the model formulation is presented here for completeness.

The model equation is a steady-state, integrated vorticity balance

$$\rho_0 g J(\xi, d) + g J(\alpha, d) - g\gamma(\nabla_H^2 \alpha + \rho_0 \nabla_H^2 \xi)$$

$$+ \hat{\mathbf{k}} \cdot \nabla \times \tau_s = 0, \quad (1)$$

where ξ is the sea surface elevation, d bottom depth, ρ_0 a reference density, g the acceleration of gravity, α the vertically integrated density $[= \int_{-d}^{0} \rho dz$, where z is the vertical coordinate positive upward and zero at the surface], γ a bottom friction parameter equivalent to the bottom Ekman layer thickness and given a value of 500 cm, τ_s the surface wind stress vector, and $J(a, b) = (\partial a/\partial x)(\partial b/\partial y) - (\partial a/\partial y)(\partial b/\partial x)$ is the Jacobian operator, with x positive to the east and y positive to the north.

Eq. (1) specifies the complete vorticity balance represented in the model and is solved for surface elevation ξ using a finite-element technique (Galt, 1980). Input data (d, α, τ_s) are specified at the vertices of the triangular grid elements in the model domain, which is small enough so that f is considered constant. The first term of (1) represents the vorticity contribution from the interaction of the barotropic field with bottom topography. The second is the contribution from the interaction of the baroclinic field with the bottom. The third term represents vorticity input in the bottom Ekman layer due to frictional coupling of the baroclinic and barotropic modes with the bottom. Finally, the last term gives the vorticity input due to the curl of the surface wind stress.

3. Boundary conditions

To find the solution to (1) it is necessary to specify the surface elevation ξ around the perimeter of the model domain. Available technology does not allow for direct measurement of ξ to the necessary precision required and as a result an indirect estimation of the barotropic field must be utilized. As originally applied by Galt (1975) the barotropic boundary conditions were estimated from wind stress data and then adjusted. Han et al. (1980) showed that current meter observations taken along the boundaries can be used to determine the barotropic/geostrophic mode along the perimeter of the model domain. The model perimeter for the Georgia shelf application is composed of four boundaries: a shallow inner along-shelf boundary defining the coastline, a deep outer along-shelf boundary, and northern and southern cross-shelf boundaries connecting the inner and outer boundaries. The inner-shelf boundary has the stringent requirement that there be no net transport

through the coastline. The boundary conditions here are determined by summing the Ekman, baroclinic, and bottom frictional transport components perpendicular to the boundary segments and setting them equal and opposite to the barotropic transport. This results in a $\nabla\xi$ along the coast necessary to balance the transports such that there is no net flux through the inner-shelf boundary.

To determine the barotropic mode around the remainder of the model perimeter, Han et al. developed a technique using averaged velocity measurements from current meters positioned along the northern and southern cross-shelf boundaries to construct a smooth horizontal profile of geostrophic velocity perpendicular to the cross-shelf boundaries. The geostrophic relation

$$\hat{\mathbf{k}} \times \mathbf{u}_g(z) = - \frac{g}{f} \left(\nabla\xi - \frac{h}{d} \frac{\nabla\alpha}{\rho_0} \right) \quad (2)$$

is then used to obtain $\nabla\xi$ along these two boundaries. In the above equation $\hat{\mathbf{k}} \times \mathbf{u}_g(z)$ represents the component of geostrophic velocity perpendicular to a boundary segment, h is the current meter depth, and d is the total depth of the water column. This procedure, however, produces only elevations relative to other points along the boundaries. To produce the absolute boundary elevations, we set the nearshore station on the northern boundary to 10 cm, which is an arbitrary value because only elevation gradients are required. Then ξ is determined along the nearshore boundary by satisfying the no-flux condition. Using the end points of the inner-shelf boundary we now integrate $\nabla\xi$ along the southern and northern cross-shelf boundaries. The outer boundary values are found by interpolating between the outer endpoints of the two cross-shelf boundaries.

Having specified the boundary conditions, (1) is used to solve for the barotropic mode in the interior of the model domain. However, these prescribed boundary conditions will not necessarily produce the best possible flow field. The formulation of the model is such that continuity must be satisfied. In general, specification of ξ around the entire model boundary is an over-specificiation of the boundary conditions and can lead to errors in the barotropic transport field. The model responds to an excess or deficit of transport through the boundaries by veering the barotropic interior flow near the southern boundary so that the bottom Ekman transport satisfies the continuity condition. A discussion of this effect is included in Galt (1980). The final tuning of the model is accomplished by fixing ξ on the northern boundary and computing several solutions of (1) with different slopes on the outer boundary until a bottom flow that is parallel to the isobaths is obtained in the vicinity of the southern boundary. This iteration process changes the values of ξ on the southern boundary but

the values of $\nabla\xi$ are held constant except at the boundary segment adjacent to the point defining the coast. However, changes in the absolute ξ field along the southern boundary (which result from varying the slope on the outer boundary) only affect the flow in a narrow band north of the southern boundary.

After solving (1) for the ξ field, a geostrophic velocity profile is determined for each triangular element by superimposing the barotropic and baroclinic profiles. The barotropic current is uniform from surface to bottom whereas the baroclinic profile is assumed to have a linear vertical shear. Transports per unit width are computed by vertically integrating the geostrophic profiles and superimposing surface and bottom Ekman transports.

4. Input data

The Galt model was applied to the Georgia shelf using current meter and hydrographic data collected during July 1977 (Lee, 1980; Atkinson et al., 1979).

Location of the current meter moorings is shown in Fig. 1. Current and temperature measurements were obtained 17 m below the surface and 3 m above the bottom using Aanderaa current meters at the 30 m (moorings A and G), 45 m (mooring F) and 75 m (moorings B, D and E) isobaths. Five transects of CTD stations perpendicular to the coastline were obtained by Skidaway Institute of Oceanography during 4–8 July 1977 (Fig. 2). These stations define the vertices of the triangular grid used in the model (Fig. 3). Three fictitious density stations were included in the grid between the Jacksonville and St. Simons transects in order to avoid very elongated triangles. This was done by interpolating the α and depth fields between the transects. Station depths used in the model ranged from about 15 m at the inshore stations to about 65 m at the deep stations. For reasons to be discussed later, our attempts to include stations with depths exceeding 65 m gave poor results. Wind data were obtained from the Sa-
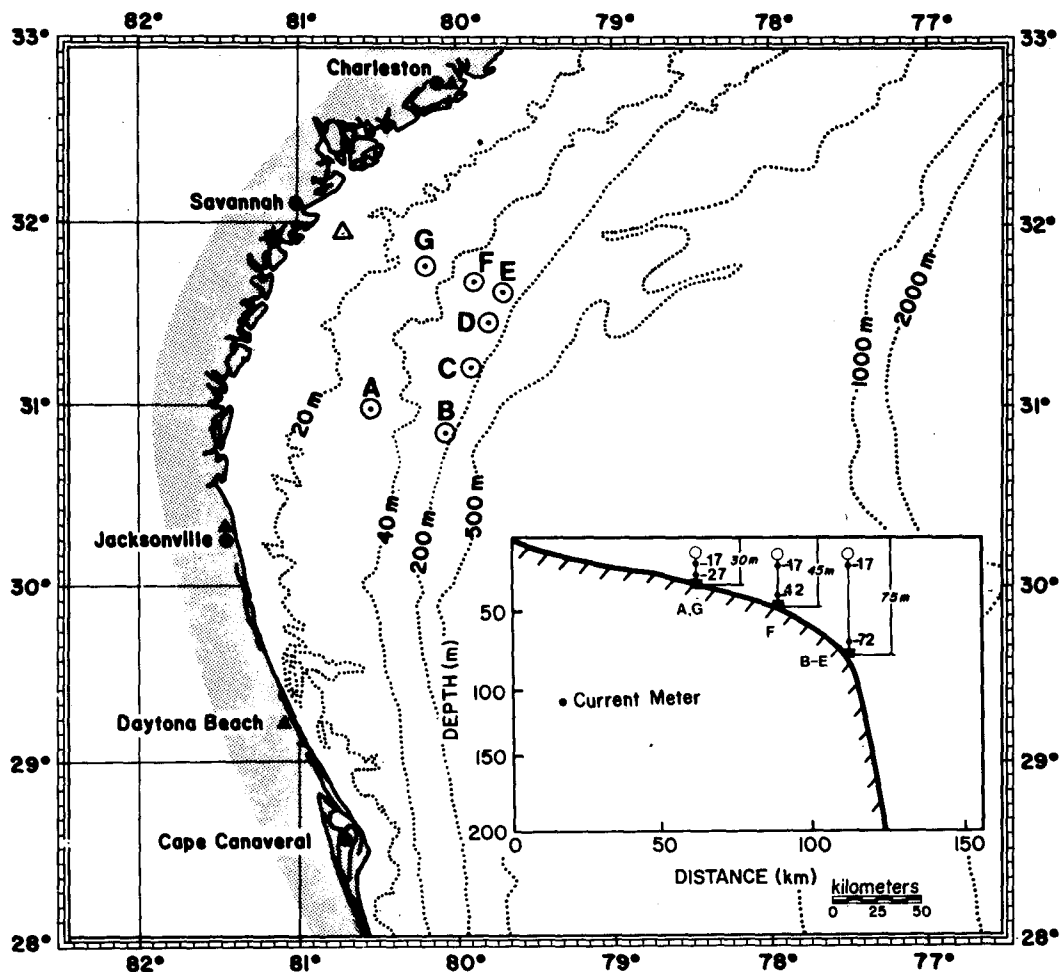

FIG. 1. Location of current meter moorings A–G (⊙) and coastal sea level (▲) and wind stations (●) for the period 2 July to 10 November 1977.
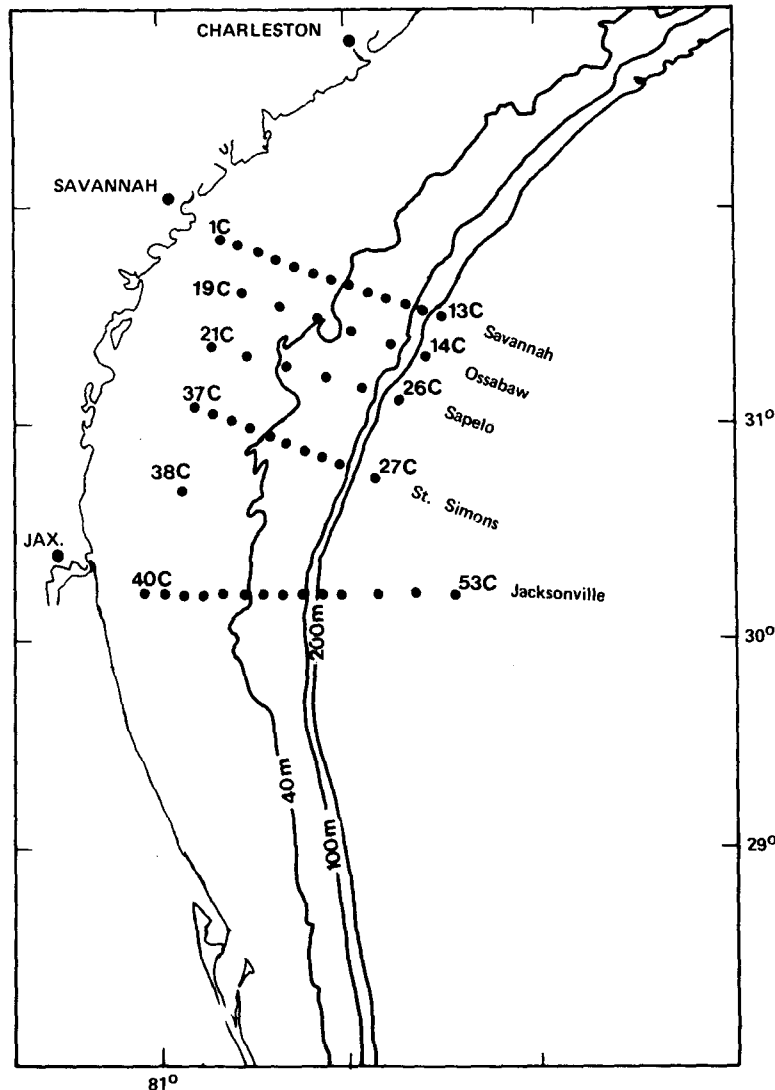
FIG. 2. Hydrographic station locations 4–8 July 1977 from Atkinson et al. (1979).
Stations are shown by solid dots, and only the start and end stations of each transect
are numbered.

vannah Light Tower located in the northwest corner of the model domain (Blanton et al., 1979).

The original current records were filtered to suppress tidal fluctuations using a 40 h low-pass Lanczos filter and rotated 30° into an isobath-oriented coordinate system where north is 30° T and east is 120° T. The resulting time series from the 17 m depth for the four-month summer period are shown in Fig. 4. Also shown are coastal sea level from Daytona Beach, Florida, and Charleston, South Carolina, and local winds. The sea level data were "adjusted" to remove the static effect of atmospheric pressure.

Low-frequency currents indicate that the shelf can be separated into two distinct flow regimes according to the physical processes controlling variability: in

the outer shelf (water depths > 40 m) subtidal flow variability appears to be primarily produced by Gulf Stream forcing (transient wave-like meanders and eddies); and in the mid- to inner-shelf (water depths ≤ 40 m) wind forcing has a significant influence on low-frequency flow variability (Lee et al., 1981). Density forcing may also be important in the inner shelf off Georgia and north Florida due to river discharge, which forms a low-salinity, alongshelf band over the inner 10–20 km of the shelf (Blanton and Atkinson, 1978).

The influence of the Gulf Stream is clearly seen in data from the 75 m isobath (shelf break: moorings BT, DT and ET). Current amplitudes in the upper layer ranged from ±40 to ±80 cm s^{-1} about a mean northward flow of 55 cm s^{-1} (Fig. 4). Energetic cur-
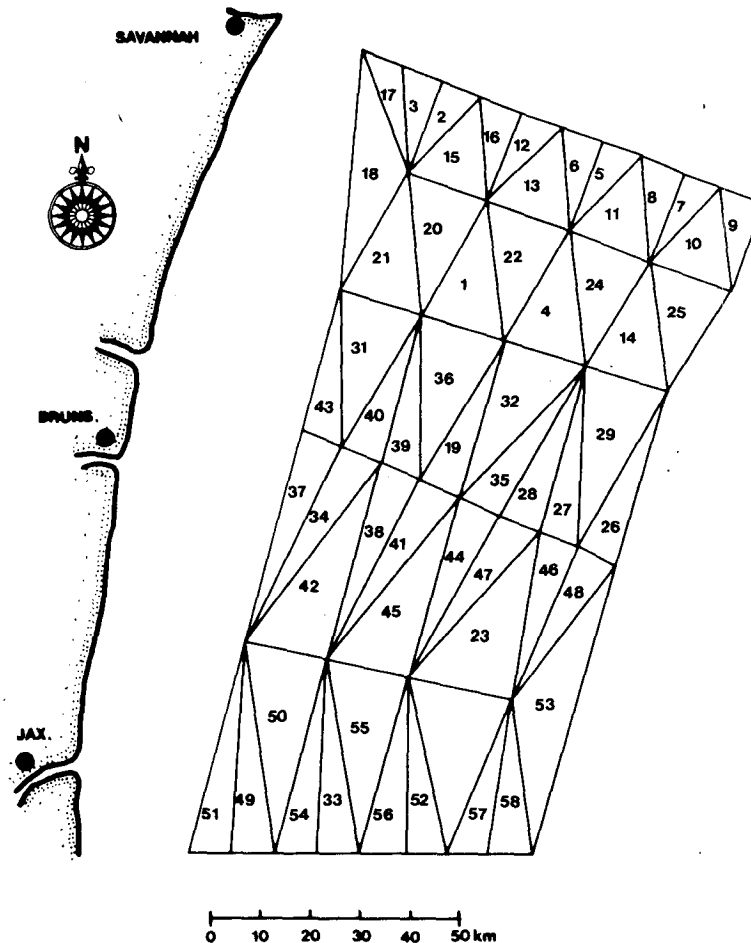
FIG. 3. Triangular grid of model domain, deep stations excluded.
Numbers are for element identification.

rent fluctuations produced broad-banded spectral peaks (not shown) at periods of 2.3, 3.5, 5 and 10 days that were coherent between the cross-shelf (u) and alongshelf (v) components, with the cross-shelf leading by 90° in phase, suggestive of propagating wave motion. Downstream current meter pairs of the summer experiment revealed northward propagation of subtidal velocity and temperature fluctuations that were coherent over the 90 km alongshelf array spacing at periods of 5–12 days in the upper layer. South-ward propagation was observed in both upper and lower layers at periods of 2–3 days. Temperature fluctuations with amplitudes ranging from ±2 to ±4°C were significantly coupled to the velocity variations. Largest temperature changes occurred in the lower layer. Current and temperature fluctuations were coherent over the 55 m vertical instrument separation at periods of 2–2.5 days.

Lee *et al.* (1981) have shown that cyclonic cold-core eddies forming along the Gulf Stream front make up a major component of the low-frequency current and temperature variability over the Georgia

outer shelf during all seasons in the 2-day to 2-week period band. The occurrence of an eddy has been observed to produce a cyclonic perturbation of the mean northward flow coupled to a sharp decline in the temperature (Fig. 4, events 4–11). The influence of eddies on the velocity and density fields can extend 35–40 km shoreward from the shelf break. Down-stream dimensions of these features can reach 100–200 km in the region from Jupiter, Florida, located 170 km south of Cape Canaveral, to Charleston, South Carolina.

Gulf Stream meanders have been observed to produce onshore-offshore displacements of the surface front ±15 km from the shelf break in the Georgia shelf region (Bane and Brooks, 1979). These mean-ders are believed to be produced by waves traveling to the north at about 40 cm s⁻¹ with wavelengths of 100–200 km and periods of ~10 days (Legeckis, 1979; Niiler and Mysak, 1971; Orlanski, 1969).

Low-frequency current fluctuations at the 30 m isobath (mid-shelf) were highly coherent and nearly in phase over the 90 km array separation distance
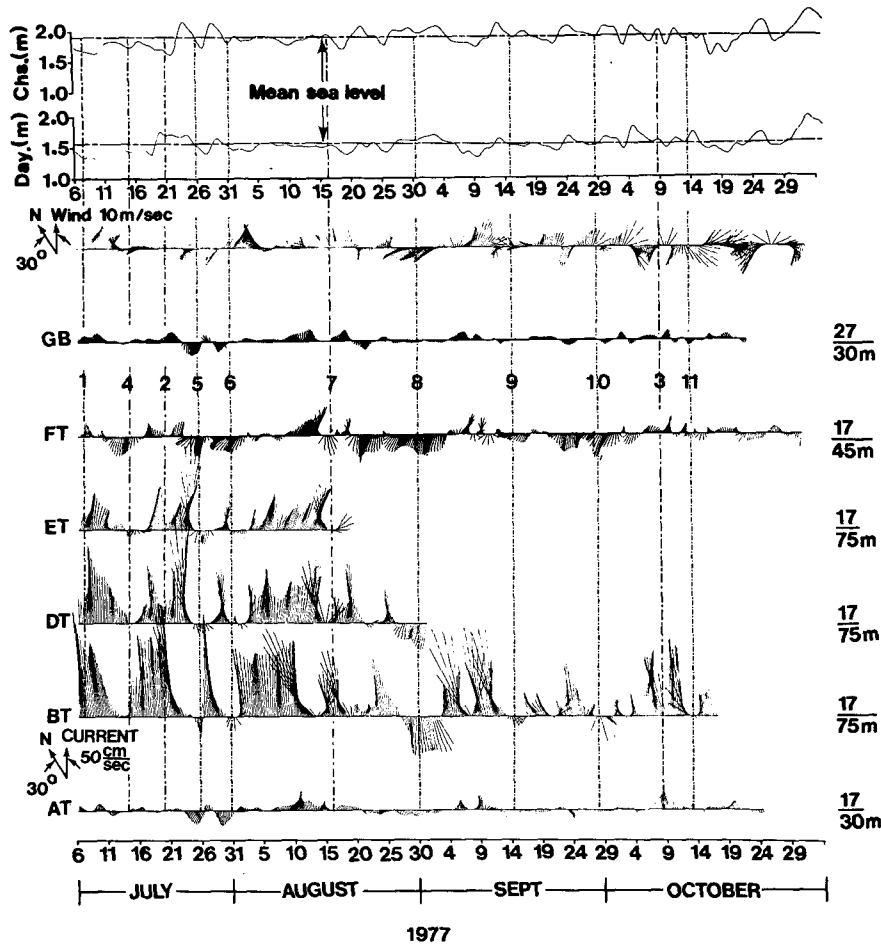
FIG. 4. Time series of 6 h rotated current and wind vectors, and corrected sea level from Charleston (Chs.) and Daytona (Day.), using 40 h low-pass filtered records for 6 July to 31 October 1977. Sea level corrected for atmospheric pressure by 1 mb pressure = 1.01 cm sea level. Magnitude and rotation of vectors are shown by scale arrows on left. Instrument depth and water depth are shown on right. Vertical lines are for meander and eddy event identification.

[Fig. 4; also see Lee et al. (1981)]. Current amplitudes ranged from ±10 to ±40 cm s^{-1} with little vertical shear, indicating a barotropic fluctuation. Current variations were also significantly correlated with local winds and coastal sea level changes. Northward (southward) winds, which were coherent over alongshelf distances of 600 km in this region[2], lead coastal sea level set-down (set-up) at Daytona and Charleston by about 12 h and northward (southward) currents at moorings A and G by about 20 h. Thus at mid-shelf a significant fraction of the subtidal current variability appears to be largely in response to wind-induced cross-shelf sea level slopes. Northward winds produce an offshore surface Ekman transport which causes coastal sea level to set-down, creating a cross-shelf pressure gradient that drives a northward barotropic alongshelf flow. The opposite response occurs with southward winds.

A similar coastal sea level and current response to local wind forcing was found for winter conditions on the New England shelf by Beardsley and Butman (1974) and Scott and Csanady (1976); on the Georgia shelf during winter by Lee and Brooks (1979) and Tebeau and Lee (1979); and on the Washington shelf by Hickey and Hamilton (1980).

A blow-up of the subtidal current vectors over a 17-day period that includes the hydrographic cruise dates (4–8 July 1977) are shown in Figs. 5 and 6. The hydrographic data are shown in Fig. 7. It is apparent from these data that the outer shelf was under the influence of a Gulf Stream disturbance during the period of the hydrographic cruise. On 4 July the Gulf Stream front was located offshore of the shelf break at Savannah and upwelling appears

---

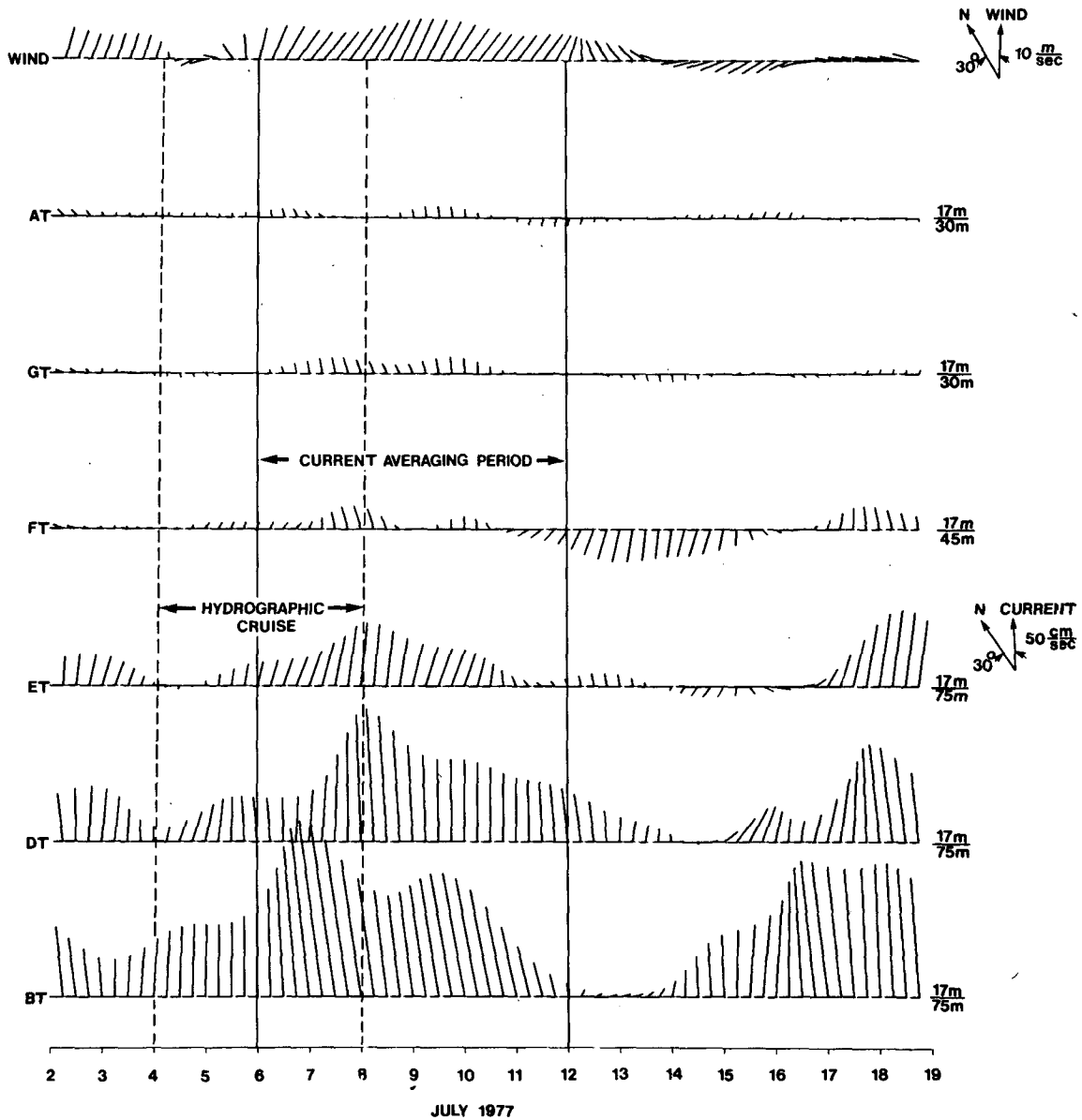[2] Hamilton, 1981, unpublished report to Bureau of Land Management.

FIG. 5. Blow-up of 6 h current vectors for 2-18 July, top meters.

to have occurred along the bottom due to the presence of uplifted cold temperatures. A flow reversal occurred at the 45 and 75 m isobaths in the lower layer where the mean flow is weak. In the upper layer where the northward mean is strong there was a decrease in northward speeds. There also appears to be more freshwater in the inner shelf off Savannah than in the sections to the south, presumably due to run-off from the Savannah River. At the Ossabaw section, 20 km to the south, on 5 July the front was slightly closer to the shelf break and flow conditions were similar to those observed at the Savannah section. However at the St. Simons section the Gulf Stream front was located shoreward of the shelf break on 6 July which appears to have produced the strong northward flow in the upper and lower layers at the 75 m isobath (current meters BT and BB) and increased temperatures along the slope. On 7 and 8 July off Jacksonville the Stream edge was again observed offshore and upwelling is indicated by the colder temperatures at the shelf break. Following the offshore meander at Jacksonville a large decrease in current speed was observed from 7 to 12 July off St. Simons in the upper and lower layer and appeared to produce the observed current reversal off Savannah (FT and ET) from 12 to 16 July.

The above observations were most likely produced by a northward propagating wave in the Gulf Stream
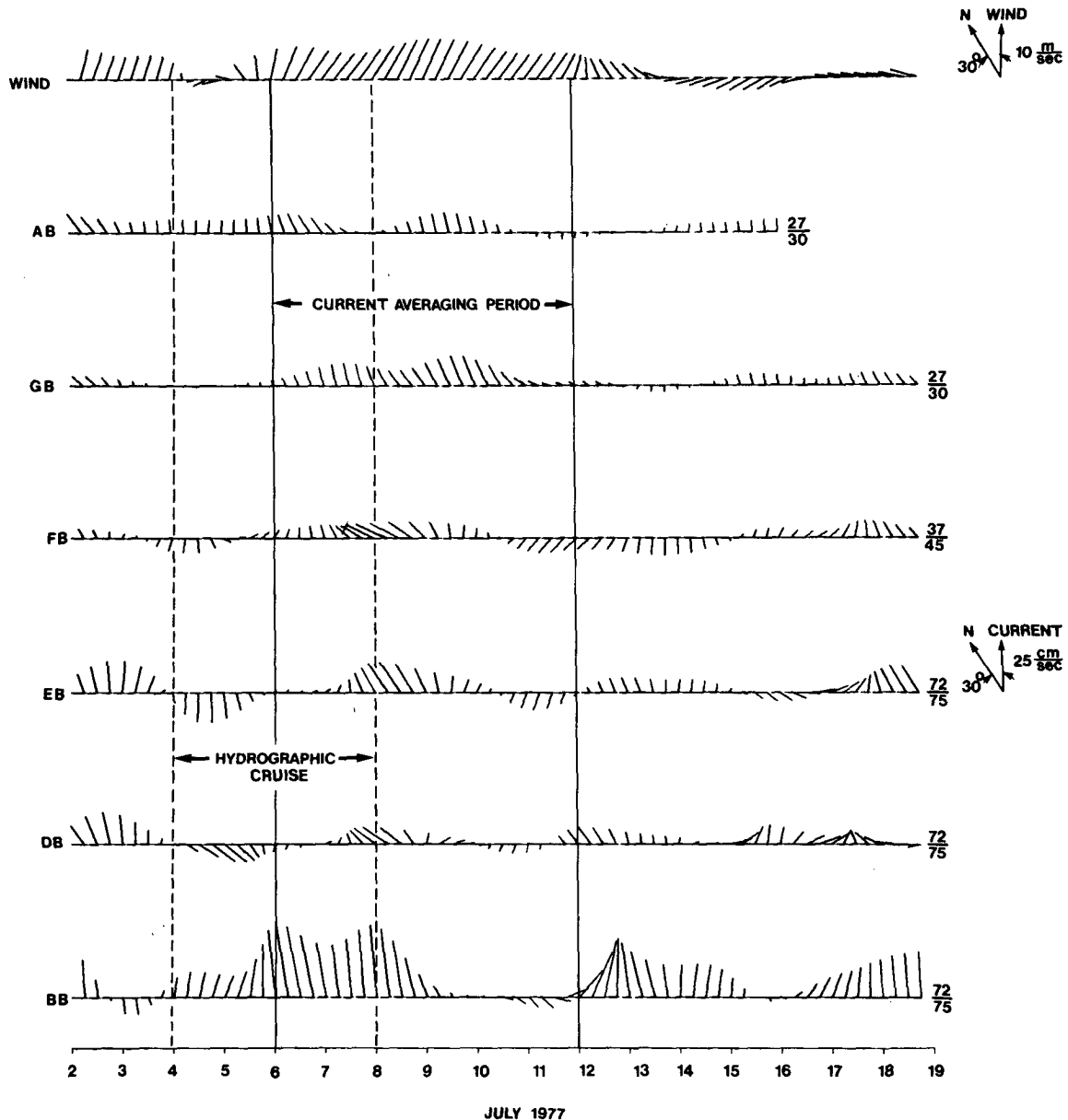
FIG. 6. Blow-up of 6 h current vectors for 2–18 July, bottom meters.

front. The phase speed of this wave was estimated with the current meter data to be approximately 46 cm s^{-1} to the north. The wavelength was roughly estimated from the hydrographic data to be about 160 km. The wave period of the disturbance is estimated from the wave speed and length to be about four days. These wave properties are in close agreement with those estimated by Legeckis (1979) from satellite images and may be a type of unstable continental shelf wave that is advected northward by the strong current in the Gulf Stream.

At the mid-shelf locations (30 m isobath) the subtidal flow appears to be relatively unaffected by the wave motions at the shelf break during the period of the hydrographic measurements. The velocity fluctuations are strongly barotropic even though the shelf is vertically stratified and significant visual correlation with the wind is indicated.

In order to use the current meter data to determine the sea surface slope boundary conditions for the model and later for model evaluation, low-frequency variations occurring on time scales of several days were removed by averaging the low-passed velocities over a six-day period beginning 6 July. The resulting six-day averages (geostrophic velocities) for the bottom meters at locations E, F and G (Fig. 1) were
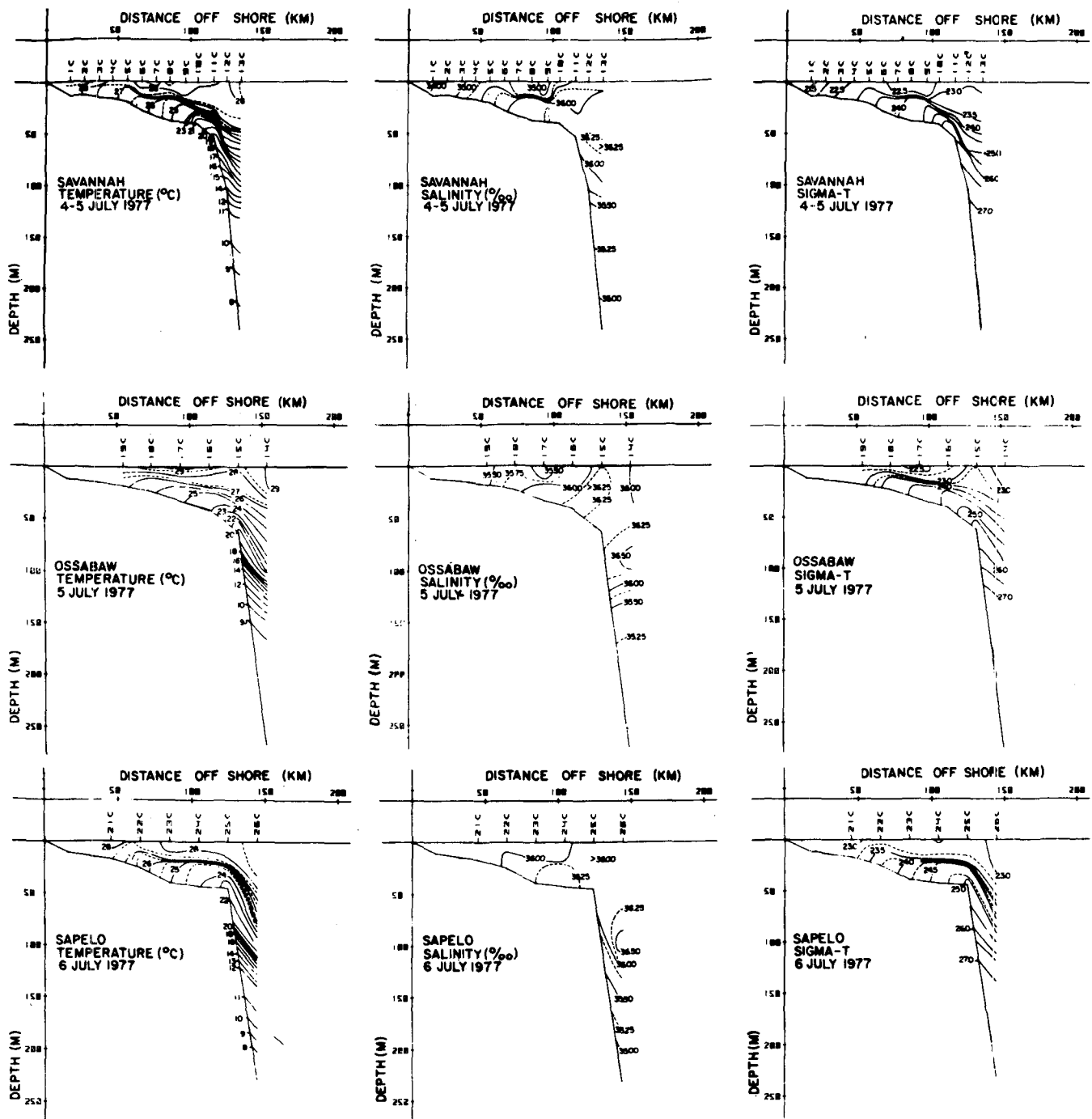
FIG. 7a. Transects of temperatures (°C), salinity (‰) and density (σ_t) off Savannah, Ossabaw and Sapelo, Georgia (see Fig. 2 for locations).

used to determine the boundary conditions, i.e., surface elevations along the northern boundary using Eq. (2).

Velocity data along the southern boundary were not available. Instead, the surface slope along this boundary was estimated by using the geostrophic bottom velocity data from the A and B bottom meters which are actually located in the central portion of the grid. The lack of appropriate velocity data for determining the southern boundary conditions is expected to somewhat degrade the model results. However, as was pointed out earlier, the model solution is dominated by the input along the northern boundary. Therefore, improper specification of the slope
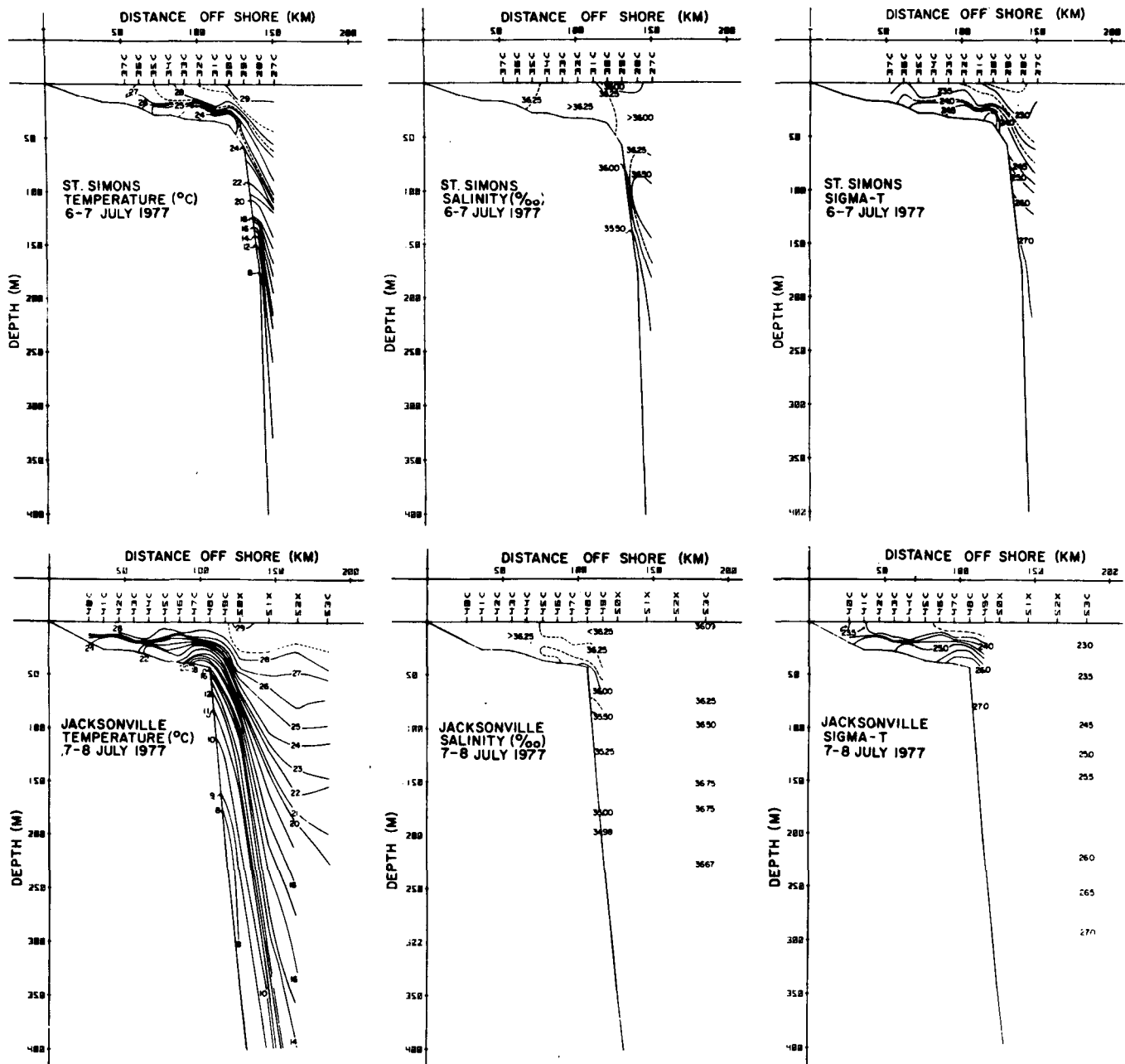
FIG. 7b. Transects of temperatures (°C), salinity (‰) and density (σ_t) off St. Simons, Georgia, and Jacksonville, Florida (see Fig. 2 for locations).

along the southern boundary is expected to only affect the solution in the triangles adjacent to this boundary.

5. Model results

The initial application of the Galt model to the Georgia shelf included the deep hydrographic stations made seaward of the shelf break where the cross-shelf depth gradient increases by an order of

magnitude over that of the mid-shelf-region (Figs. 1 and 2). The diagnosed velocity field at 20 m and near bottom is shown in Figs. 8 and 9, respectively, along with the six-day average observed velocities. The predicted velocities at the shelf break appear to have no relation to observed velocities nor does the general pattern match the remainder of the model domain. The only agreement is in the bottom velocities at mid-shelf.
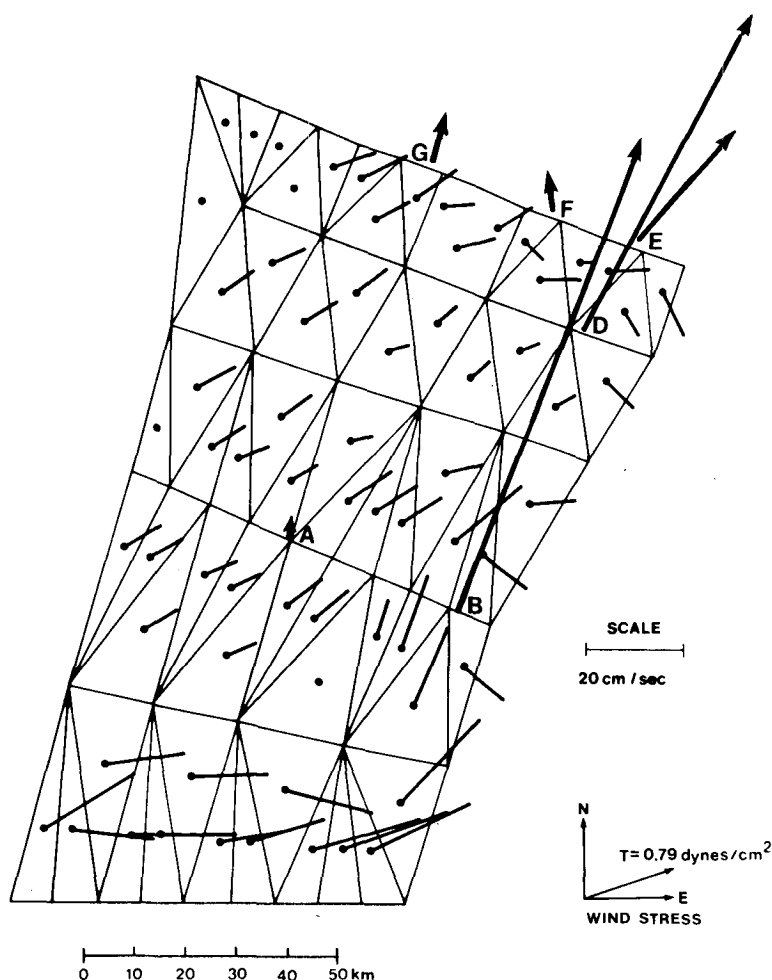
The diagnosed velocity field in the deep regions

FIG. 8. Diagnosed velocity at 20 m including deep hydrographic stations.
Averaged current meter velocities are indicated by heavy arrows.

is clearly anomalous and can be traced to two causes. The first is a resolution problem. In evaluating $J(\alpha, d)$ in the vorticity equation, the model must compute relatively small differences between large quantities, i.e., $(\partial\alpha/\partial y)(\partial d/\partial x) - (\partial d/\partial y)(\partial\alpha/\partial x)$. Recall that α is the vertically integrated density, so that the model is required to produce horizontal gradients of α between shallow and deep stations. Therefore, in regions of rapid depth change closely spaced stations are required to adequately determine the horizontal gradient of α. The second difficulty arises from lack of the synopticity in the hydrographic data. In the deeper shelf break regions, the vertical and horizontal density field is strongly influenced by transient Gulf Stream disturbances so that significant changes can occur on a time scale of 1–2 days. As a result a steady-state model will not properly diagnose a realistic velocity field over the deep regions of the model domain, which is strongly time dependent.

In view of these difficulties it was decided to restrict the model domain to the region shoreward of the 65 m isobath where the depth gradient is small and the density field changes more slowly. Figs 10, 11, and 12 show the effect of omitting the deep stations on the depth field, the α field in terms of vertically averaged σ_t, and the diagnosed ξ field, respectively. The α field in Fig. 11 was obtained by fitting a third-order polynomial to the α versus depth relationship. The field was then smoothed by requiring all values to be less than or equal to one-half standard deviation from the polynomial fit. Both the measured density field and predicted surface elevation distribution showed significantly larger cross-shelf gradients than along-shelf. The predicted sea surface elevation stands about 3–4 cm higher at the outer shelf compared to the inner shelf, with very little along-shelf variation. The vertically averaged density field indicates an along-shelf variation in the

outer shelf due to the Gulf Stream disturbance mentioned earlier and cross-shelf gradients over the mid- to inner-shelf. Discharge from the Savannah River appears responsible for the increased cross-shelf density gradient in the northwest corner of the grid.

In computing vertical velocity profiles there is an additional difficulty due to the assumption of a constant vertical eddy diffusivity K, which is unrealistic for the region in question. Downward penetration of momentum induced by wind stress is not expected to be constant since vertical stratification varies over the model domain. Therefore the water column was divided into two layers above and below the pycnocline depth for each grid triangle by taking the average pycnocline depth for the three stations comprising a triangle. The Ekman transport was computed from τ_s/f and τ_b/f for the surface and bottom layers respectively. The baroclinic velocity profile was determined from the density distribution, and combined with a constant barotropic velocity derived from the sea surface slope to obtain the geostrophic profile.

Figs. 13, 14 and 15 show the results of modeling the velocity field at the surface, 20 m and bottom. The measured currents are also shown at 20 m and near bottom and compared to the predicted values in Table 1. As expected there is rather poor agreement between observed flow at the shelf break (moorings B, D and E) and the diagnosed flow due to the Gulf Stream influence over the outer shelf. However, the results look more promising for the mid-shelf region.

The surface velocity field was computed from the combination of surface Ekman and barotropic velocity components (Fig. 13). Surface currents are primarily wind driven, in an offshore direction $\sim 30°$ to the right of the wind. The predicted currents at 20 m and bottom in the mid-shelf region are quite similar in magnitude and direction and agree reasonably well with the measured flow. These levels are either within or below the pycnocline at mid-shelf (Fig. 7) and are also below the surface Ekman layer depth (h_E) which is estimated at ~ 10 m from $h_E = 0.1\rho^{-1} f^{-1} \tau_s^{1/2}$ (Csanady, 1976). Thus the flow below the pycnocline (lower level) results only from the combined effects of barotropic (sea surface slope) and baroclinic (horizontal density gradient) forcing. The observed flow is northward, parallel to the isobaths, and with little vertical shear, which indicates that the cross-shelf gradient of surface elevation ($\partial\xi/\partial x$) was the main driving force of the lower layer flow.

6. Volume transport

Volume transport into and out of the model domain was computed for both the upper and lower
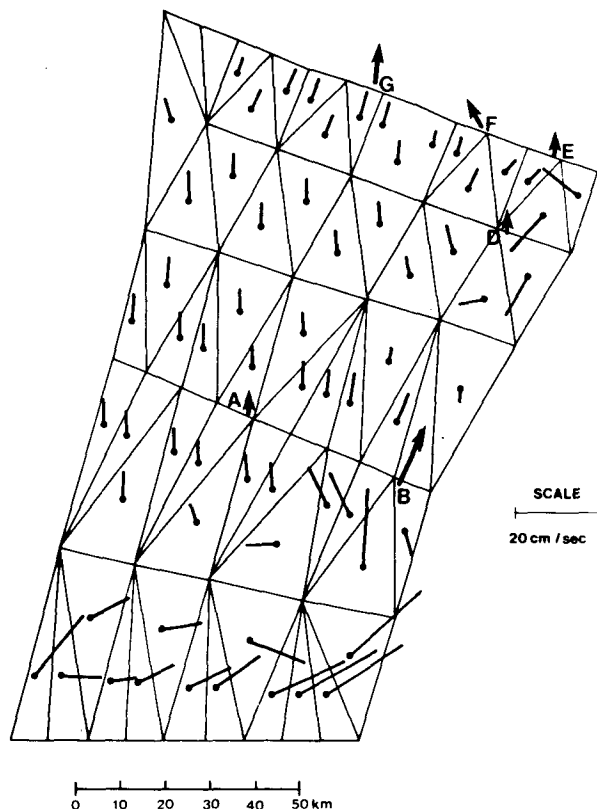

FIG. 9. Diagnosed bottom velocity including deep hydrographic stations. Averaged current meter velocities are indicated by heavy arrows.

layers and total water column. Transport in the upper layer was computed by vertically integrating the geostrophic velocity profile from the surface to the pycnocline and combining with the surface Ekman transport. For the lower layer, the velocity profile, composed of geostrophic plus bottom Ekman components, was vertically integrated from the pycnocline depth to the bottom. The transport per unit width for the upper and lower layers are shown in Figs. 16 and 17 respectively. Transport through the south, outer and north boundaries was determined for each layer by multiplying the length of the boundary triangle segments by the component of transport perpendicular to the segment. The component of the transport due to barotropic and baroclinic modes and the surface and bottom Ekman layers was computed separately. The results are given in Table 2 along with total transports through the model boundaries.

The total transport indicates a net northward flow with an offshore component. The offshore component was produced largely by offshore transport in the upper layer of 123×10^3 m^3 s^{-1} that was only partially balanced by an onshore transport in the lower layer of 38×10^3 m^3 s^{-1}. Cross-shelf flow in the upper layer was primarily due to an offshore Ekman trans-
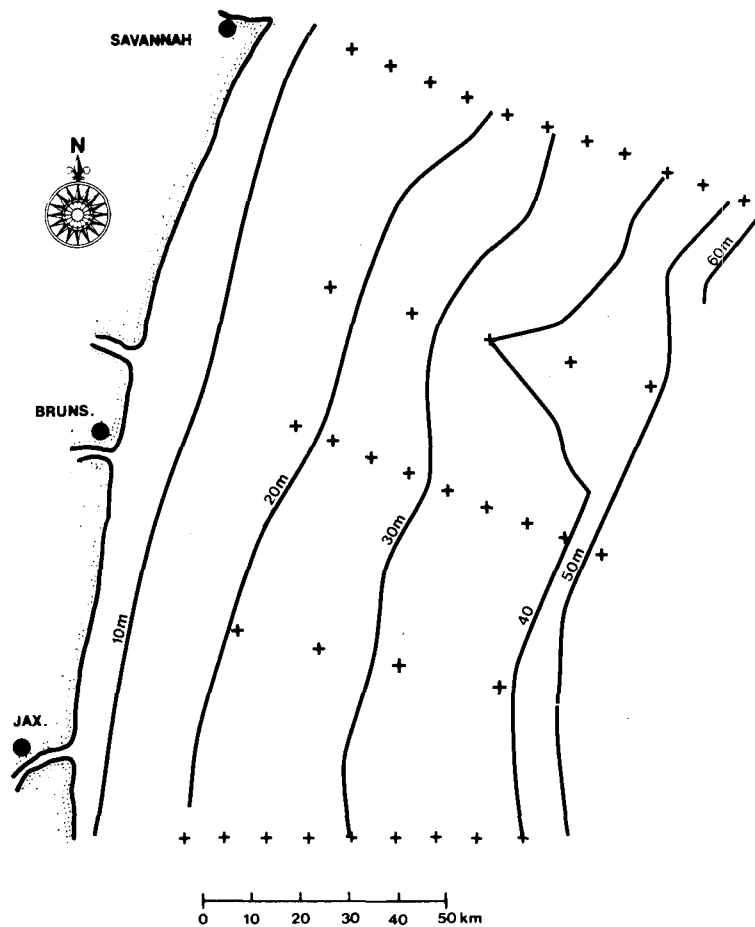
FIG. 10. Depth field used in model excluding depths greater than 65 m.

port of 120×10^3 m^3 s^{-1}. Along-shelf flow in the upper layer was complicated by a significant northward barotropic component ranging from about 70 to 100 $\times 10^3$ m^3 s^{-1} that was opposed by a southward Ekman transport of about 70×10^3 m^3 s^{-1} and a southward baroclinic component of about 30×10^3 m^3 s^{-1}, which appears to have been an effect of Savannah River freshwater discharge for it only acts at the northern boundary. These flows were superimposed to produce the complex upper layer transport pattern (Fig. 16).

Transport in the lower layer was more uniform and consistent than in the upper layer (Fig. 17). Transport in this layer was northward at about 50 to 60×10^3 m^3 s^{-1} and on-shore at 38×10^3 m^3 s^{-1}. Along-shelf transport in the lower layer was northward and almost totally barotropic, ranging from 70 to 80×10^3 m^3 s^{-1}. The baroclinic along-shelf transport was insignificant in the lower layer. Cross-shelf transport in the lower layer occurred primarily in the bottom Ekman layer as an onshore barotropic flow of 85×10^3 m^3 s^{-1} that appears to be a consequence of the frictional interaction of the northward baro-

tropic flow. This onshore barotropic transport was partially opposed by an offshore baroclinic component in the bottom boundary layer of 42×10^3 m^3 s^{-1}, which appears to be much larger than could reasonably be expected from the weak southward lower layer baroclinic transport and is therefore questionable.

The baroclinic transports appear to be weak, except for localized effects near the Savannah River, and are also somewhat questionable in the bottom Ekman layer along the outer boundary. If we neglect the baroclinic transport then the total volume transport is to the north at about 70×10^3 m^3 s^{-1} and offshore at 40×10^3 m^3 s^{-1}. The upper layer part of the total transport is offshore at 120×10^3 m^3 s^{-1} and northward at about 10×10^3 m^3 s^{-1}. In the lower layer the transport is northward at about 60×10^3 m^3 s^{-1} and onshore at 80×10^3 m^3 s^{-1}. By dividing the lower layer transport by the average cross-sectional area gives an average northward velocity of about 4.5 cm s^{-1} which agrees well with the observed bottom velocities (Table 1).

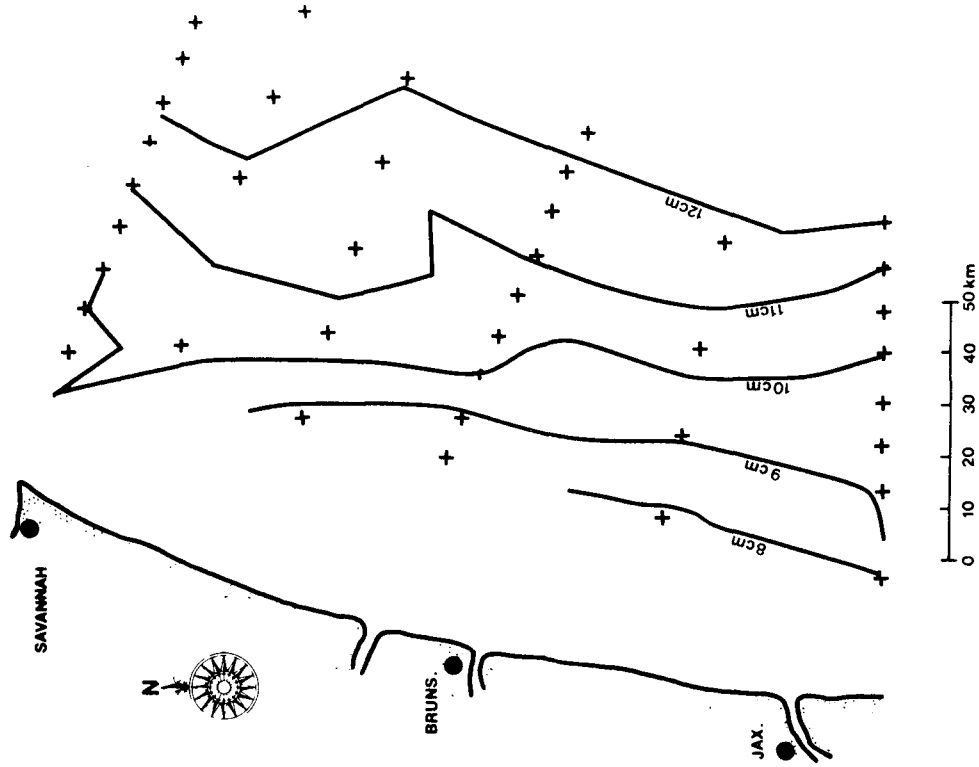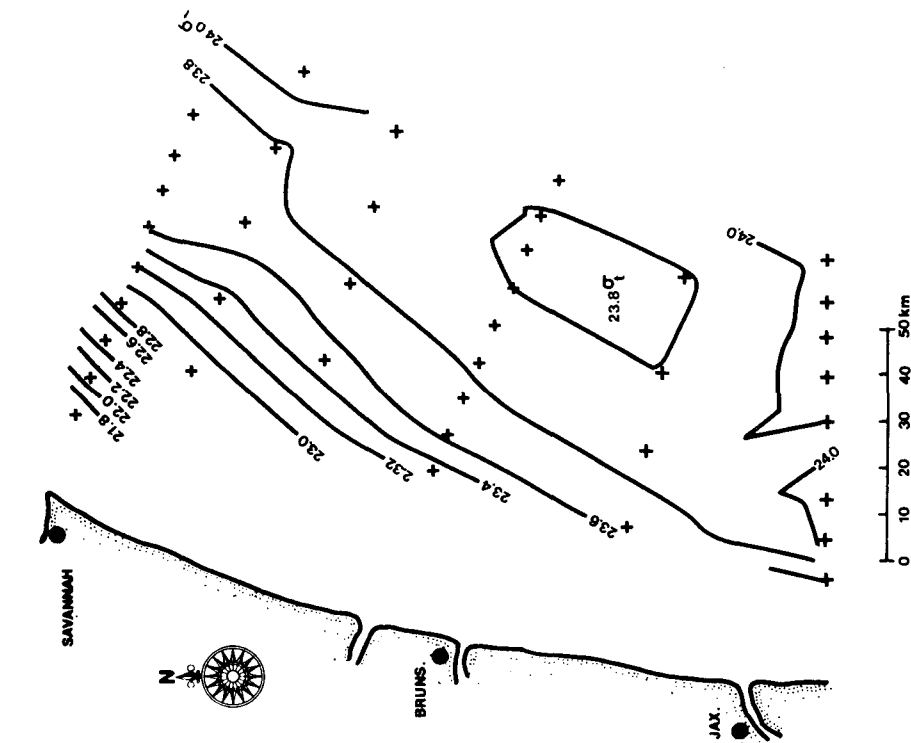FIG. 12. The diagnosed surface elevation (ξ) field representing the solution to the vorticity equation (1). Depths greater than 65 m have been excluded.
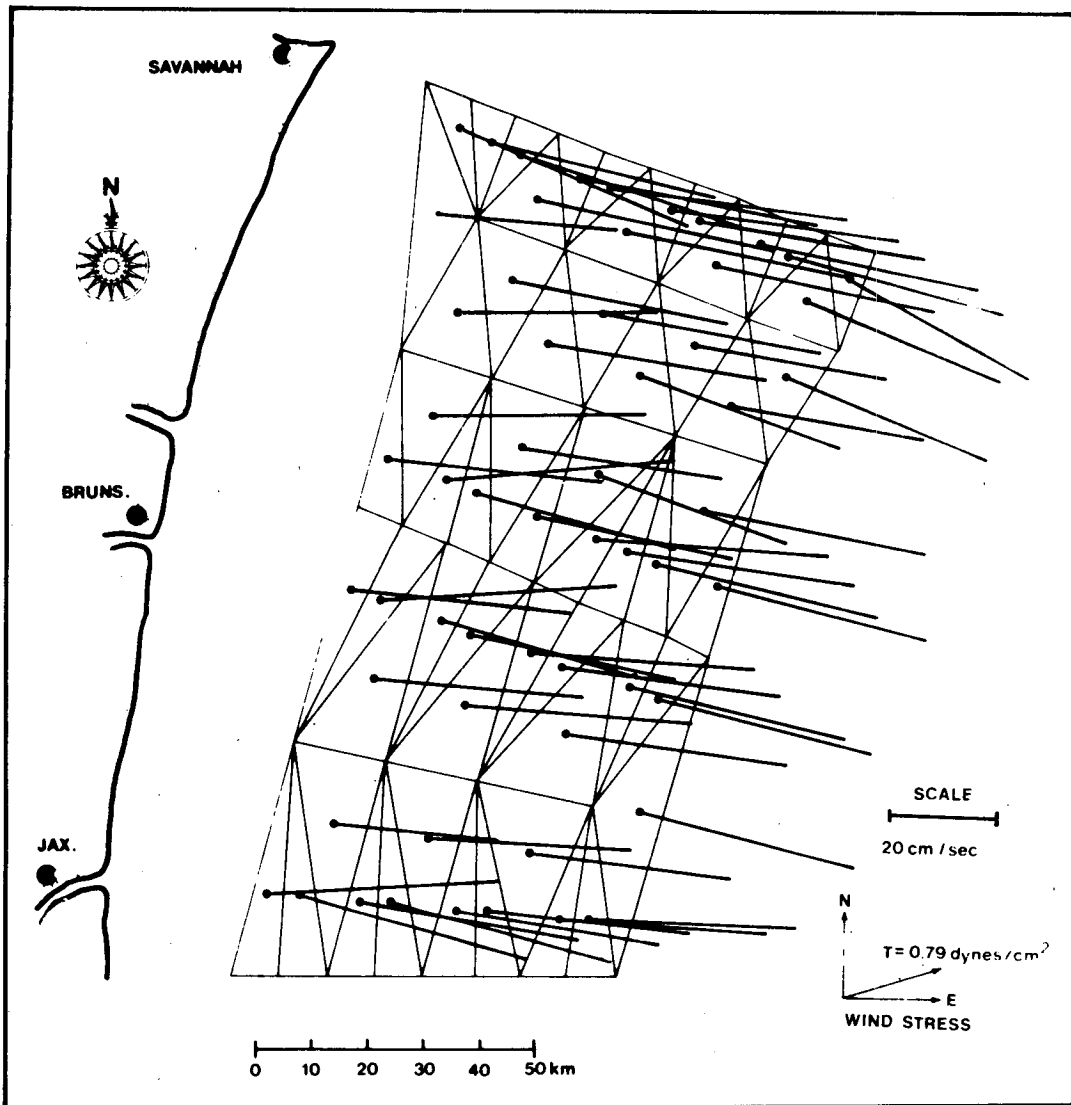
FIG. 11. Vertically averaged density (α) expressed in terms of σ_t. Alpha has been smoothed to a standard deviation of 0.5. Depths greater than 65 m have been excluded.

FIG. 13. Diagnosed surface velocities with stations deeper than 65 m excluded.

TABLE 1. Comparison of diagnosed velocity components (cm s^{-1}) to six-day non-rotated velocity averages from top and bottom current meters (hydrographic stations deeper than 65 m have been excluded).

| Current meter | Water depth (m) | Triangle number* | Bottom** | | | | Top** | | | |
| | | | Observed velocity | | Modeled velocity | | Observed velocity | | Modeled velocity | |
			u	v	u	v	u	v	u	v
A	30	19	0.1	4.7	−0.4	4.5	0.2	2.9	−1.4	4.6
B	75	53	7.4	12.7	4.4	6.9	38.8	97.7	4.4	6.9
D	75	25	−0.4	2.7	0.4	4.3	36.1	65.9	0.4	4.3
E	75	9	−0.1	4.1	1.8	4.6	20.7	23.9	1.8	4.6
F	45	7	−3.1	5.2	1.2	3.1	−0.6	6.7	1.2	3.1
G	30	6	0.3	9.0	3.7	7.2	2.3	8.7	3.7	7.2

* Triangle numbers specify triangular grid elements in Fig. 3.
** Top meter is located 17 m below surface; bottom meter is 3 m above bottom.

FIG. 15. Diagnosed bottom velocity field with stations deeper than 65 m excluded. Averaged current meter velocities are indicated by heavy arrows.
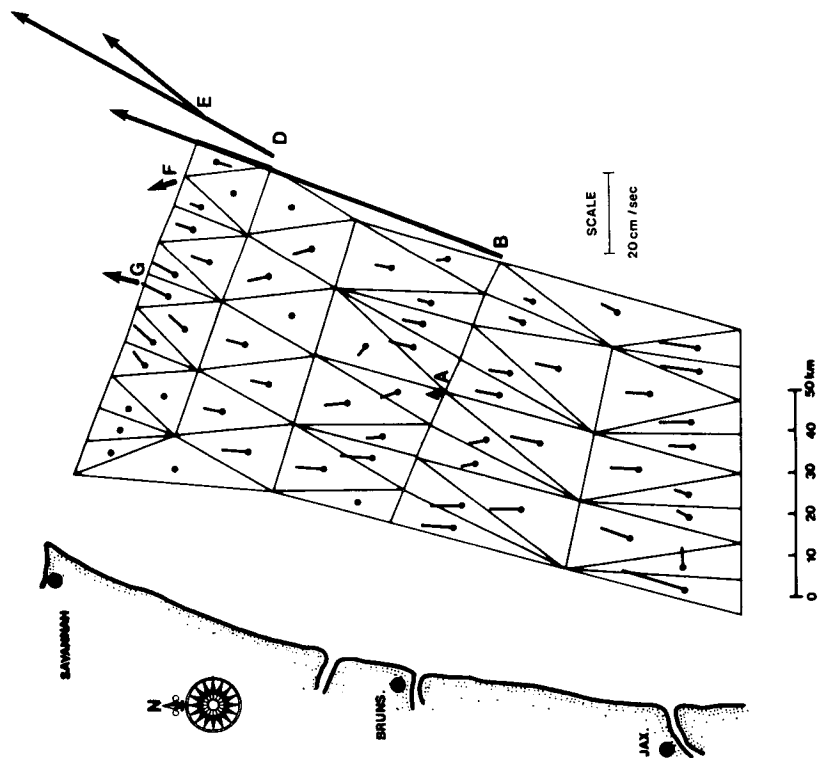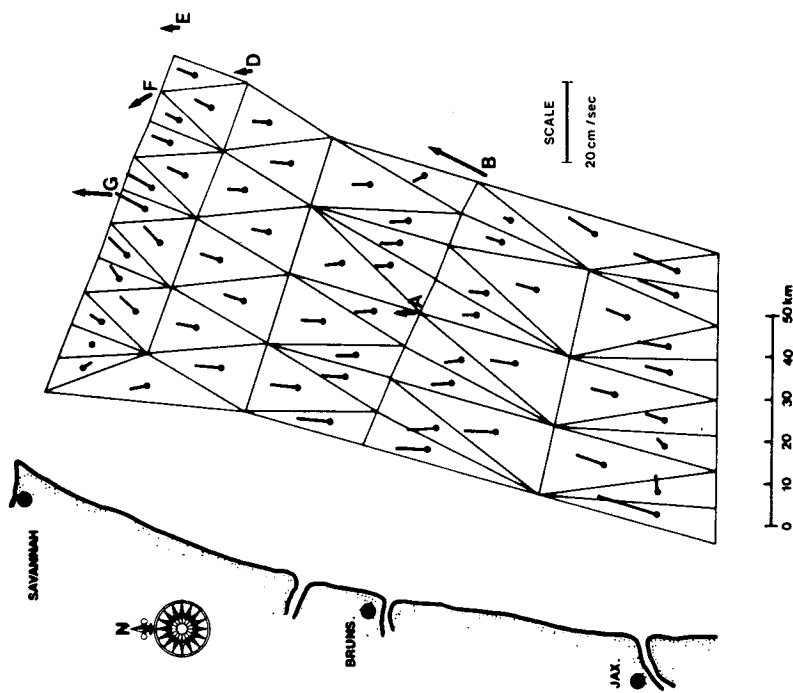
FIG. 14. Diagnosed velocities at 20 m with stations deeper than 65 m excluded. Averaged current meter velocities are indicated by heavy arrows.
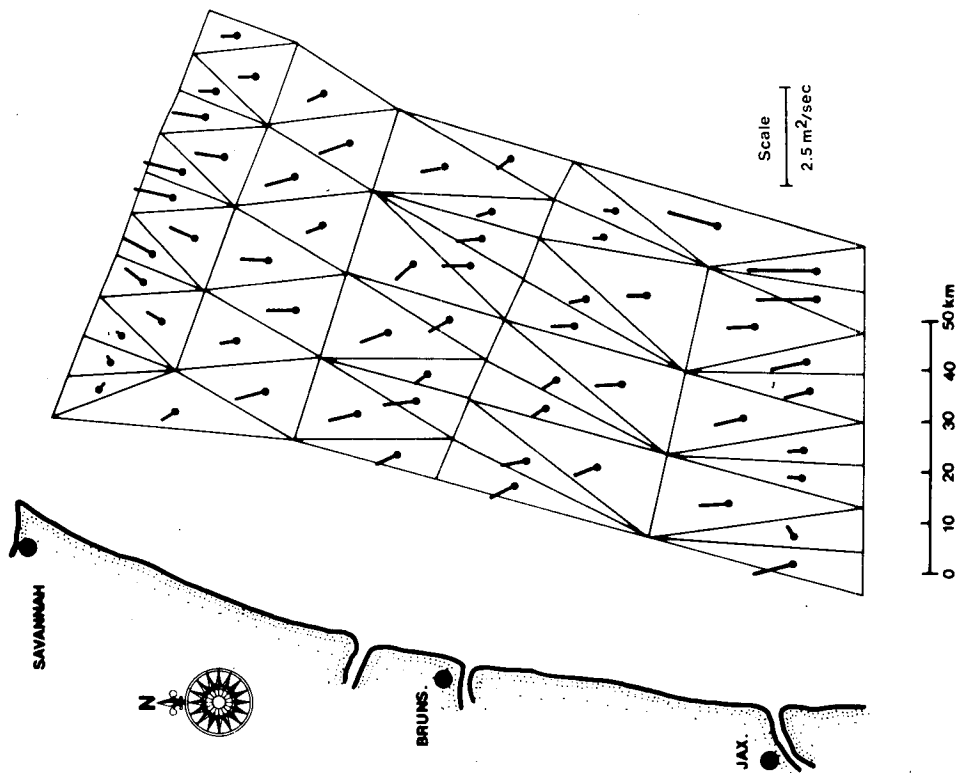
FIG. 17. Transports per unit length for lower layer. Stations deeper than 65 m are excluded.
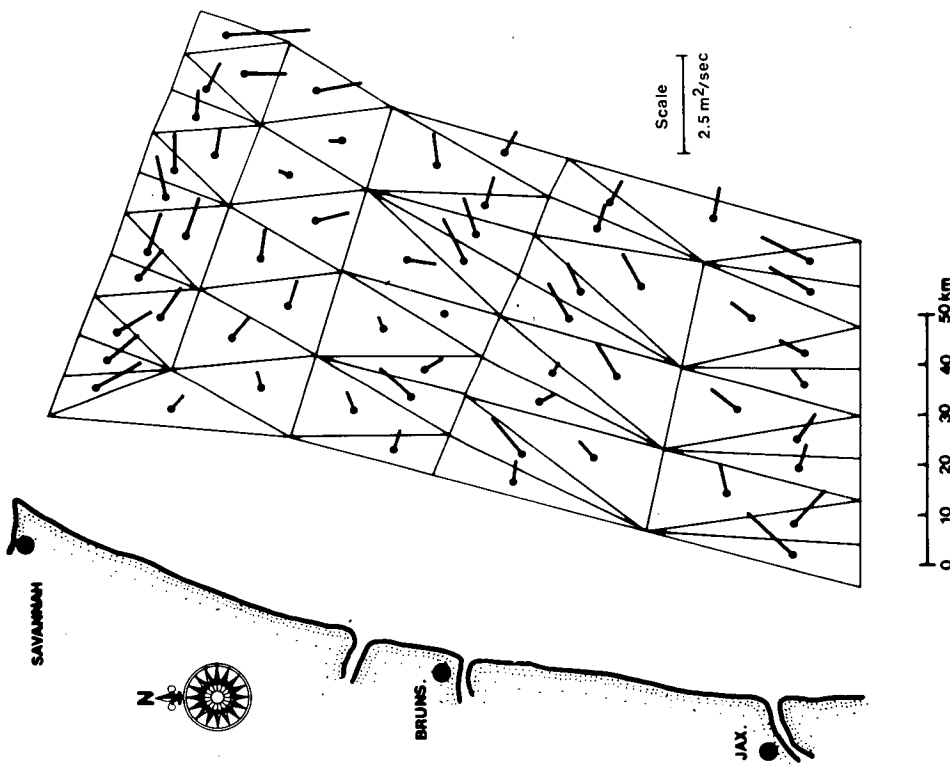

FIG. 16. Transports per unit length for upper layer. Stations deeper than 65 m are excluded.

TABLE 2. Volume transports ($\times 10^3$ m^3 s^{-1}) through the boundaries of the model domain for top and bottom layers (minus indicates flow into the domain and plus is for outward flow).

Volume transport	Boundaries		
	South	Outer	North
Top barotropic	−100.4	−0.4	+66.2
Bottom barotropic	−80.6	+6.6	+67.0
Total barotropic	−181.0	+6.2	+133.1
Top baroclinic	+0.3	+2.8	−32.2
Bottom baroclinic	−0.2	−1.5	−3.5
Total baroclinic	+0.2	+1.3	−31.6
Top Ekman	+73.0	+120.8	−69.1
Bottom Ekman barotropic	+9.3	−85.0	−23.4
Bottom Ekman baroclinic	+7.7	+42.0	+9.6
Total top layer	−27.1	+123.2	−35.1
Total bottom layer	−63.7	−38.0	+49.7
Total transport	−90.8	+85.2	+14.6

The total cross-shelf transport of 40×10^3 m^3 s^{-1} in the offshore direction is equivalent to a net exchange rate and can be used to estimate the shelf residence time. The volume of shelf water within the model domain (excluding depths greater than 50 m) and including the shallow waters west of the domain to the coast (Fig. 10) is approximately 40×10^{10} m^3. Therefore the shelf residence time is estimated at 3.8 months, which agrees reasonably well with the 2.5 month estimate of Atkinson et al. (1978).

7. Conclusions

Application of the Galt diagnostic model was found to be useful for prediction of mean flow conditions in the Georgia mid-shelf region. The model is not applicable to the outer-shelf region for two reasons:

1) The transient occurrence of Gulf Stream disturbances (meanders and eddies) on time scales of two days to two weeks produce large temporal and spatial variations in the density and flow fields that strongly alias results from a steady-state model. To resolve this problem would require two to three ships making quasi-synoptic three-dimensional maps of density every day for one month. These data could be time-averaged to produce a mean density field that should be more representative of the mean baroclinic flow over the outer shelf.

2) Depth increases rapidly at the continental slope, making it difficult to resolve horizontal derivatives of the vertical averaged density. To overcome this problem would again require an increased number of hydrographic stations.

Galt (1975) also mentions that the model is not applicable to shallow regions where the surface and bottom Ekman layers merge, which indicates that the model is probably not useful for depths < 20 m.

Thus on the Georgia shelf the model is limited to predicting mean flows in the mid-shelf region where the water depth ranges from 20 to 40 m.

Model results indicate that wind forcing is a major mechanism driving mean flows at mid-shelf. Wind forcing occurs in two ways that are directly coupled: 1) in the upper layer wind-driven Ekman transports produced the largest component to the cross-shelf flow and a significant amount of the along-shelf flow; and 2) cross-shelf Ekman transports can cause coastal sea level variations that result in mean cross-shelf sea level slopes and barotropic along-shelf flows. The barotropic flow accounts for a significant portion of the mean along-shelf transport in the upper layer and practically all of the along-shelf transport in the lower layer. The baroclinic component of the transport due to cross-shelf and along-shelf density gradients appears to be insignificant in the lower layer and only marginally significant to along-shelf flow in the upper layer.

The model predicts a six-day average along-shelf volume transport of 70×10^3 m^3 s^{-1} toward the north between the 20 and 50 m isobaths. In the summer 86% of this flow occurs below the pycnocline due to the controlling effect of the barotropic mode in the lower layer. The net cross-shelf transport is offshore at 40×10^3 m^3 s^{-1} for the six-day period and is equivalent to a volume exchange rate. The shelf residence time is estimated from this exchange rate at 3.8 months.

The Galt model could be made to be more applicable to the Georgia shelf if it were modified to include variations in time, and coupled the sea level response directly to surface wind stress.

REFERENCES

Atkinson, L., J. O. Blanton and E. Haines, 1978: Shelf flushing rates based on the distribution of salinity and fresh water in the Georgia Bight. *Coastal Estuar. Mar. Sci.,* 7, 464–472.
——, A. Edwards, J. Singer, W. Chandler and G. Paffenhofer, 1979: Hydrographic observations in the Georgia Bight (July 1977). Georgia Marine Science Center, University of Georgia, Skidaway Island, Tech. Rep. No. 79-3, 126 pp.

Bane, J. M., Jr., and D. A. Brooks, 1979: Gulf Stream meanders along the continental margin from the Florida Straits to Cape Hatteras. *Geophys. Res. Lett.,* **6,** 280–282.

Beardsley, R. C., and B. Butman, 1974: Circulation on the New England continental shelf: response to strong winter storms. *Geophys. Res. Lett.,* **1,** 181–184.

Blanton, J. O., and L. P. Atkinson, 1978: Physical transfer processes between Georgia tidal inlets and nearshore waters. *Estuarine Interactions,* J. Wiley, Ed., Academic Press, 512–532.

——, L. Bailey, D. Hayes and A. S. Dicks, 1979: Oceanographic and meteorological data 15 km off the coast of Georgia. Skidaway Institute of Oceanography, Data Rep. 2, 56 pp.

Csanady, G. T., 1976: Mean circulation in shallow seas. *J. Geophys. Res.,* **81,** 5389–5399.

Galt, J. A., 1975: Development of a simplified diagnostic model for interpretation of oceanographic data. NOAA Tech. Rep. ERL 339-PMEL 25, 46 pp.

——, 1980: A finite element solution procedure for the interpolation of current data in complex regions. *J. Phys. Oceanogr.,* **10,** 1984–1997.

——, and G. Watabayashi, 1977: Use of a diagnostic circulation model to study shelf circulation. NOAA/PMEL unpublished report.

Han, G. C., D. Hansen and J. A. Galt, 1980: Steady-state diagnostic model of the New York Bight. *J. Phys. Oceanogr.,* **10,** 1998–2020.

Hickey, B. M., and P. Hamilton, 1980: A spin-up model as a diagnostic tool for interpretation of current and density mea-

surements on the continental shelf of the Pacific northwest. *J. Phys. Oceanogr.,* **10,** 12–24.

Lee, T. N., 1980: Summary of subsurface current measurements on the Georgia shelf (Dec. 1976–Nov. 1977). Tech. Rep. UM RSMAS 80001, University of Miami, 88 pp.

——, and D. Brooks, 1979: Initial observations of current, temperature and coastal sea level response to atmospheric and Gulf Stream forcing. *Geophys. Res. Lett.,* **6,** 321–324.

——, L. P. Atkinson and R. Legeckis, 1981: Detailed observations of a Gulf Stream spin-off eddy on the Georgia continental shelf. *Deep-Sea Res.,* **28,** 347–378.

Legeckis, R., 1979: Satellite observations of the influence of bottom topography on the seaward deflection of the Gulf Stream off Charleston, South Carolina. *J. Phys. Oceanogr.,* **9,** 483–497.

NOAA–NESS, 1974: Experimental Gulf Stream analysis, NOAA-2 Satellite Thermal Infrared (VHRR). U.S. Department of Commerce, Environmental Products Group, F.O.B. No. 4, Room 3301, Washington, DC 20233.

NAVOCEANO, 1975: Experimental ocean frontal analysis charts. U.S. Naval Oceanographic Office, Code 3710, 1975–1977.

Niiler, P. P., and L. A. Mysak, 1971: Barotropic waves along an eastern continental shelf. *Geophys. Fluid Dyn.,* **2,** 273–378.

Orlanski, I., 1969: The influence of bottom topography on the stability of jets in a baroclinic fluid. *J. Atmos. Sci.,* **26,** 1216–1232.

Scott, J. T., and G. T. Csanady, 1976: Nearshore currents off Long Island. *J. Geophys. Res.,* **81,** 5401–5409.

Tebeau, P., and T. N. Lee, 1979: Wind-induced circulation on the Georgia Shelf (winter 76/77). Tech. Rep. UM RSMAS 79003, University of Miami, 177 pp.